Generation and control of monodisperse bubble suspensions in microgravity

Pau Bitlloch[a], Xavier Ruiz[b,f], Laureano Ramírez-Piscina[c,f], Jaume Casademunt[a,d,e,f]

[a]*Departament d'Estructura i Constituents de la Matèria, Universitat de Barcelona, 08028-Barcelona, Spain*
[b]*Departament de Química, Física i Inorgànica, Universitat Rovira i Virgili, 43007-Tarragona, Spain*
[c]*Departament de Físca Aplicada, Universitat Politècnica de Catalunya, 08028-Barcelona, Spain*
[d]*Departament de Física de la Matèria Condensada, Universitat de Barcelona, 08028-Barcelona, Spain*
[e]*Universitat de Barcelona Institute of Complex Systems, Universitat de Barcelona, 08028-Barcelona, Spain*
[f]*Institut d'Estudis Espacials de Catalunya, 08034-Barcelona, Spain*

Abstract

A new experimental setup for the generation of homogeneous, monodisperse bubble suspensions in turbulent duct flows in microgravity has been designed and tested in drop tower experiments. The setup provides independent control of bubble size, void fraction and degree of turbulence. The device combines several slug-flow injectors that produce monodisperse bubble jets, with a turbulent co-flow that ensures homogeneous spatial spreading. Bubble separation in the scale of the most energetic eddies of the flow, and bubble size sufficiently smaller, ensure that turbulence is most efficient as a mechanism for spatial spreading of bubbles while preventing coalescence, thus optimizing the homogeneous and monodisperse character of the suspension. The setup works in a regime for which bubbles are spherical, but sufficiently large compared to the turbulent dissipative scales to allow for two-way coupling between bubbles and carrying flow. The volume fraction is kept relatively small to facilitate particle tracking techniques. To illustrate the potential uses of the method we characterize the statistics of bubble velocity fluctuations in steady regimes and we characterize the transient relaxation of the buoyancy-driven pseudo-turbulence when gravity is switched-off.

Nomenclature

ν	Kinematic viscosity
Re	Reynolds number
U_c	Characteristic flow velocity
L_c	Characteristic system size
T_c	Characteristic time of the flow
λ_k	Kolmogorov length
τ_k	Kolmogorov time
λ_{Max}	Characteristic size of most energetic eddies
τ_{Max}	Characteristic time of most energetic eddies
τ_B	Bubble response time
Q_l	Volumetric liquid flow rate
Q_g	Volumetric gas flow rate
$Q_{\text{co-flow}}$	Volumetric co-flow rate
ϑ	Void fraction
d_T	T-junction tubes diameter
d_B	Bubble size
u_i	Component of the bubble velocity in the i direction
n	Mean number of bubbles on given interval
σ_i	Standard deviation of i component of bubble velocity
a, b, τ	Fittings parameters for bubble velocities
d	Mean separation of pair of bubbles
d_{xy}	Mean separation in the plane xy between pairs of bubbles
$d_0, v_{\text{sep}}, \mathscr{L}$	Fittings parameters for pair separations

1. Introduction

Dispersed multiphase turbulent flows are common in many engineering applications, but pose formidable challenges to fundamental theory due to the complex interplay between the inherent fluctuations of the carrier and the random distribution of the dispersed phase, together with the presence of break-up and coalescence phenomena [1, 2, 3, 4, 5]. In particular the physics of bubbles in a liquid carrier [6, 7, 8] is widely recognized as crucial for a variety of space technologies. These include for instance power generation and propulsion [9], thermal management [10, 11], or life support systems and environmental control for life in space [12, 13, 14]. Given that the presence or absence of buoyancy forces affects crucially the physics of bubbly flows, the fundamental understanding of gas dispersions in microgravity conditions becomes strategic for space technology. In addition, the study of bubbly flows in weightlessness poses important challenges of management and control [15, 16] for its study and for practical applications. In this context, the capacity to generate monodisperse bubble suspensions in the absence of buoyancy forces, with good control of parameters such as bubble size and void fraction, becomes a very promising but challenging technical problem. Technical solutions to this problem may have direct relevance to specific technologies but at the same time they will provide the means to generate adequate testing grounds for fundamental research on turbulent bubble dispersions in microgravity.

Homogeneous bubbly flows have been largely studied in the past for the case of normal gravity [17, 18, 19]. Unfortunately, there is a lack of high quality data for this kind of flows in

microgravity due to the obvious limited access to microgravity environments but in particular to the technical challenges of generating bubbles of uniform size with good control but without taking advantage of buoyancy forces. Previous studies have used for instance a hypodermic needle of 0.15 mm diameter to inject gas into a liquid co-flow that detached bubbles of typically 0.92 mm in diameter carried in a turbulent pipe of 4 cm in diameter [20]. Although this procedure allows to generate bubbles with a very precise and controlled size, it creates them at a very low rate. Despite the excellent bubble homogeneity reported, these conditions do not allow one to study the interaction between large bubble ensembles and turbulence in the spirit of the present work. Similarly, in the area of microfluidics there are well known mechanisms to generate perfectly monodisperse bubbles that would perform adequately in microgravity [e.g. 21]. However, the microfluidic environment misses the turbulence component that is present in many applications and that we are interested in here. In addition, if injected in a turbulent flow, they would typically be too small compared to the relevant turbulent scales to produce a significant effect.

In this paper we build on the previous development of a device for the injection of monodisperse bubble jets in a quiescent liquid [22, 23, 24, 25, 26, 27, 28], to design, construct and test a gravity-insensitive method that generates monodisperse, homogeneous bubble suspensions, with good and independent control on the degree of turbulence, the bubble size and the bubble density. The system is tested in microgravity by means of a series of free-fall experiments conducted in the ZARM Drop Tower at Bremen. We discuss and demonstrate the practical use of this procedure and we illustrate its functionality and performance to acquire valuable data in different situations. The set-up was designed to allow a separate control of the bubble characteristics and of the turbulent flow. The idea is to combine several injectors where a slug flow with monodisperse bubbles has been created in a capillary T-junction of liquid and gas mixing, prior to injection. The bubble diameter is close to that of the junction tubes, typically of the order of one millimeter, but can be fine-tuned through the week dependence on Weber number taking advantage of the control of the volume injection rates of both gas and liquid [22]. The Weber numbers used are sufficiently small so that bubbles are essentially spherical once injected in the carrying co-flow. However, bubbles are relatively large compared to the turbulent dissipation scale, so they may have an active coupling with the flow. The latter is a duct flow with a side of 100 mm allowing for eddies much larger than the bubble size. The bubble densities here considered are such that the the void fraction is small, typically of a few percent, to facilitate particle tracking techniques and to avoid coalescence, but the method is not limited to these small values. In our experiments, the typical bubble-bubble distance is comparable to the size of the most energetic eddies, thus favoring efficient spatial dispersion while avoiding coalescence phenomena. The void fraction can also be changed by tuning the volume rates of gas and liquid injection at the capillary T-junctions that produce the slug flows injected in the carrying co-flow, as described in [22, 23, 24]. Changing the number of such injectors, which we keep at four in all our experiments, gives additional freedom
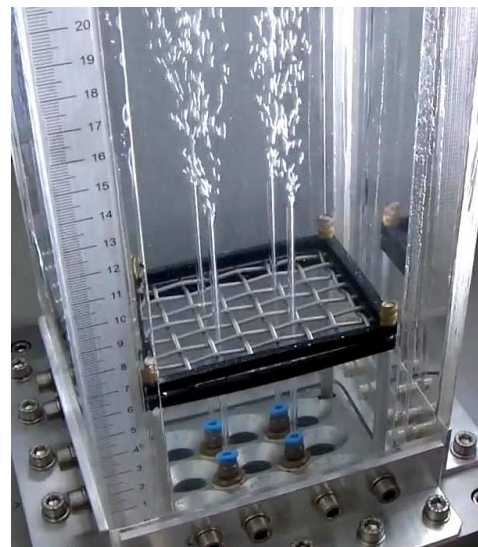

Figure 1: Snapshot of the experimental channel while injecting bubbles from the 4 injectors

to increase the void fraction further. Finally, the degree of turbulence of the carrying flow can be changed by controlling the total liquid flow rate pumped into the duct.

For illustrative purposes and to demonstrate the applicability of the set-up, we address two situations of interest. First, we use particle-tracking techniques to characterize the statistics of bubble velocities and to discuss their interaction with the flow in nearly stationary conditions. Second, we study the decay of pseudo turbulence caused by buoyancy forces in normal gravity [29, 30, 31], when gravity is switched off. In normal gravity, the decay of pseudo turbulence has been measured in the region left behind by a bubble swarm [32]. In our case we can directly visualize the process using the bubbles themselves as tracers.

The method proposed is sufficiently versatile and accurate to open many possibilities of acquiring systematic data in a variety of situations, that in turn may provide new insights into the fundamental physics of turbulent bubbly flows.

2. Experimental generation of turbulent bubble suspensions

2.1. Description of the apparatus and the protocol

To achieve a controlled homogeneous distribution of monodisperse bubbles within a turbulent flow we use a vertical duct of square section and dimensions 800x100x100 mm³. At the base of the channel we inject the carrying co-flow from nine evenly-spaced inlets (separated 30 mm between centers) with 14.5 mm inner diameter and with a final nozzle of 90° opening up to 26.9 mm diameter. Those inlets surround four bubble injectors (see Figs. 1,2) of 1.6 mm inner diameter also separated distances of 30 mm between centers. The co-flow is provided by a main water pump and split into the nine lines (one for each inlet in the duct) by using a manifold. Due to space restrictions inside the drop capsule, the main water tube suffers of a sharp 90° bending just before connecting it to the manifold producing
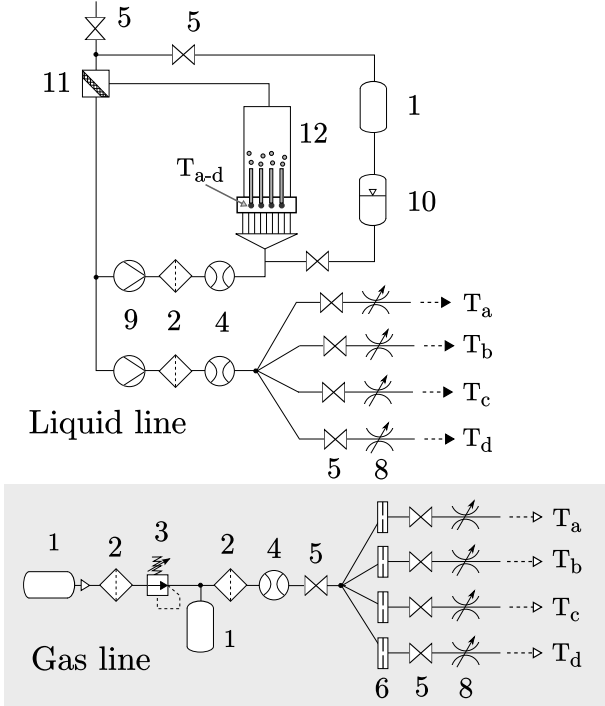
Figure 2: Sketch of the experimental setup. 1-Gas Tank, 2-Filter, 3-Pressure regulator valve, 4-Flow-meter, 5-electronic valve, 6-Precision orifice, 8-Manual throttle, 9-Liquid pump, 10-Liquid reservoir with air pressure, 11-Phase separator, 12-Experimental cell

uneven pressure distribution in it. To correct this effect we introduce a screw-ring on each outgoing line of the manifold and manually adjust their tightening on each tube in order to obtain an even flow distribution through all lines. Not correcting this effect would produce longer spatial transients in the duct before the stationary distribution of the flow was reached and even the occurrence of recirculation flows. To ensure as much as possible the required well developed turbulent co-flow conditions we locate a wire mesh (with a thickness of 2.5 mm) at the base of the duct with square holes of 10x10 mm^2, which corresponds to the characteristic scale of the most energetic eddies in steady conditions in such a duct.

Each bubble injector consists of a T-junction with capillary tubes of $d_T = 1.6$ mm, in which air and water are injected separately to generate a slug flow [22]. The outlet of the T-junction connects to a glass tube of the same inner size, allowing to inject the slug flow directly into the channel at a distance of 150 mm from the base. In this way we try to ensure the interaction between an homogeneous and well developed turbulent co-flow and the bubble jets. For the water flow entering into the T a second water pump was used. The air flow was provided by a pressure tank with a pressure regulator and, after distributed into the corresponding four lines with another manifold, has also been connected to the T-junctions. In order to obtain a controlled small gas flow for each line, it has been added one precision orifice (of typically 0.0012 in $\simeq 30.5\,\mu$m in diameter) at each air line just before the T-junction. These serve to soften large gas pressure variations into small flow changes, providing re-

ally controlled gas flows as well as a useful way to decouple the gas lines, achieving a good and independent performance of the four bubble generators. A complete sketch of the whole arrangement is presented in Figure 2.

Experiments have been performed using commercial mineral water[1]. The presence of a minimal amount of solute in the liquid has several important effects in bubbles: it increases the surface tension, making the bubbles more spherical; it produces a no-slip boundary condition at the gas-liquid interface; and it significantly decreases the probability of coalescence when bubbles collide. Note that in other experiments performed with de-ionized water, a slight deformability of bubbles of our typical size can be appreciated in the presence of buoyancy forces [33]. This deformability has a relevant role in the vicinity of the injectors, where bubbles suffer strong oscillations of their surface due to the sudden deceleration and to the large gradients of flow velocity affecting them in that region.

To record the experiments four high speed video cameras have been used: one capturing the bubble injectors, another filming the area roughly at the center of the duct, and two more at the end of the channel, recording it from two perpendicular directions.

The experimental protocol is as follows. Control parameters and flows can be adjusted and monitored during several minutes with the experimental capsule at rest, and hence with gravity. When flows are steady with the desired parameters cameras start recording. Afterward the capsule is released and micrography conditions are achieved, lasting during 4.7 s corresponding to the free fall. Due to the limited capacity of the high velocity cameras, the films are limited to approximately 8 s at a frame rate of 1000 fps. For that reason for each experiment only 3 s of bubbly flow prior to micrography is recorded. A total of 36 drops were performed. Several of them were used to test the setup and to improve and refine the injection system, and 11 drops were used for the data analysis.

2.2. Pressure compensation system

The T-junctions used to generate the slug flow injected into the cavity produce the same outcome independently of the degree of gravity due to the negligible effect of the buoyancy forces upon the process of bubble formation and detachment. Nevertheless, in our vertical configuration with the injectors located below the large mass of water filling the duct, the sudden loss of hydrostatic pressure when the micrography conditions are switched on will propagate through the system [34], producing a large change in the operating conditions in the T, and inducing a transient in its performance that may have a non negligible relaxation time, and that may have a significant effect on the very early stages of the experiment.

To minimize the effects of the transition to micrography in the bubble injectors, we have used an appropriate procedure to maintain the operating pressure in the T-junctions as constant as possible during the gravity switch-off. This is achieved by
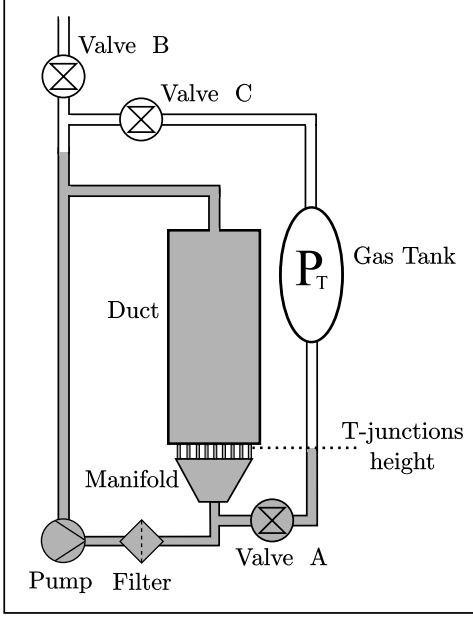
Figure 3: Schematics for the co-flow liquid line with the pressure compensation system. Gray areas represent elements filled with water while white ones are filled with air.

increasing the reference pressure in the whole system by the same amount as the hydrostatic pressure loss in the T-junctions. Figure 3 show the schematics of the main water line for the injection of the co-flow into the experimental channel. The gas tank and the three valves are used in order to compensate the pressure loss during microgravity. The specific procedure used to this aim is the following:

1. On ground, with valves "A" and "B" open, we regulate the pressure P_T in the gas tank until the water column below it reaches the height at which the T-junctions are placed. By doing that, we are setting all the air in the tank (and in its connecting tubes) at the same pressure as in the T-Junctions.

2. After adjusting the pressure in the gas tank, valve "A" is closed. From that point on, we can keep working in normal gravity conditions, but only valve "B" should remain open during this period.

3. At the start of microgravity, we close valve "B" and open valve "C" instead. In that way P_T ideally becomes the new reference pressure while the hydrostatic pressure disappears. Notice that we have kept valve "A" closed in order to prevent possible co-flow deviations through the gas tank that could happen if valves "A" and "C" were simultaneously open.

Note that some further adjustments of the initial pressure P_T on step 1 to optimize the procedure are necessary, since the sudden change of pressure in the duct during this protocol (most importantly in the superior part of the duct) will change the volume of all the present bubbles, thus producing a small flow through valve C and hence correcting the final value of P_T.

3. Experimental results

3.1. Some considerations about the duct flow

Through the present work we will describe the degree of turbulence in a duct flow by means of the Reynolds number, defined as

$$\mathrm{Re} = \frac{U_c L_c}{\nu} \, , \qquad (1)$$

with ν being the kinematic viscosity of water, U_c the characteristic velocity of the flow (its mean velocity) and L_c the characteristic size of the system (the width of a transversal section of the channel, i.e. $L_c = 100$ mm). Even though the degree of turbulence in the range of Reynolds numbers studied here is only moderate, it is convenient, as a theoretical reference, to consider the values of the relevant scaling parameters for fully developed turbulence. Table 1 shows the typical flow parameters used in our experiments, corresponding to $\mathrm{Re} = 6000$ and $\mathrm{Re} = 13000$.

Re	λ_k	λ_{Max}	τ_k	τ_{Max}	T_c
6000	0.15 mm	10 mm	22 ms	360 ms	1700 ms
13000	0.08 mm	10 mm	7 ms	170 ms	770 ms

Table 1: Scales of turbulence in a duct flow, being λ_k and τ_k the Kolmogorov scales, λ_{Max} and τ_{Max} the scales of the most energetic eddies and finally $T_c = L_c/U_c$ the characteristic time of the flow. τ_{Max} estimated using scaling relations of fully developed turbulence applied to the size of the most energetic eddy λ_{Max}

Furthermore the response time τ_B of the typical bubbles injected into the channel [35] is

$$\tau_B = \frac{d_B^2}{36\nu} \simeq \begin{cases} 70 \text{ ms}, & \text{for } d_B = 1.6 \text{ mm} \\ 170 \text{ ms}, & \text{for } d_B = 2.5 \text{ mm} \end{cases} \qquad (2)$$

Comparing the scales of turbulence in Table 1 with those associated to bubbles, seen in equation (2), we find that $\lambda_k \lesssim d_B \lesssim \lambda_{\mathrm{Max}}$ and $\tau_k \lesssim \tau_B \lesssim \tau_{\mathrm{Max}}$, implying that bubbles may be expected to exhibit an active behavior in relation to the smaller structures of turbulence and, at the same time, not produce major alterations on the main flow or on the most energetic pattern of turbulence.

The achieved void fraction ϑ of gas injected into the channel can be calculated by

$$\vartheta = \frac{4Q_g}{4Q_l + 4Q_g + Q_{\mathrm{co\text{-}flow}}} \, , \qquad (3)$$

where Q_l and Q_g stand, respectively, for the liquid and gas flow rate injected at each one of the four equivalent T-junctions. Q_{coflow} is the total liquid flow rate through the nine inlets. The value of the void fraction $\vartheta \leqslant 0.5\%$ is quite small, pointing in the direction of a limited impact of bubbles into the main structure of turbulence. This value is even smaller for the initial bubbles, which have been injected during normal gravity conditions and for which buoyancy forces have increased the distance between them.
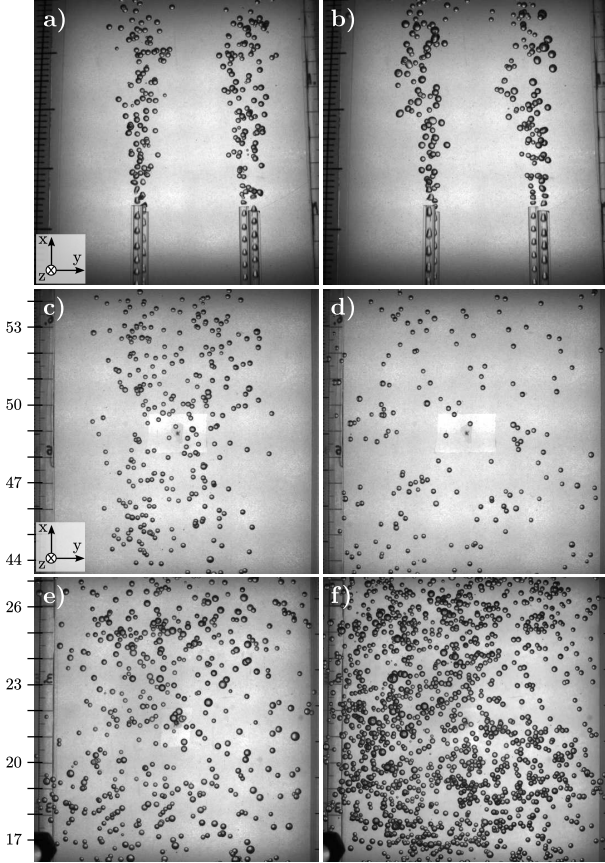
4

Figure 4: Snapshots for experiments with $Q_l = 70\frac{ml}{min}$ and $Q_g = 46\frac{ml}{min}$ ($d_B \simeq$ 1.6mm) from each injector. Scale in cm measures distance from the point where bubbles are injected. Cases *(a)-(e)* correspond to Re = 13000, while *(f)* is for Re = 6000. *(a):* Injection in 1g. *(b):* Injection in μg. *(c):* Bubbles in 1g. *(d):* Bubble suspension in μg of bubbles injected during 1g conditions. *(e)&(f):* Bubble suspension of bubbles already injected in μg conditions

Figure 5: Snapshots for experiments with $Q_l = 18\frac{ml}{min}$ and $Q_g = 46\frac{ml}{min}$ ($d_B \simeq$ 2.5mm) from each injector. Scale in cm measures distance from the point where bubbles are injected. Cases *(a)-(e)* correspond to Re = 13000, while *(f)* is for Re = 6000. *(a):* Injection in 1g. *(b):* Injection in μg. *(c):* Bubbles in 1g. *(d):* Bubble suspension in μg of bubbles injected during 1g conditions. *(e):&(f):* Bubble suspension of bubbles already injected in μg conditions

3.2. Qualitative observations

When bubbles are injected under normal gravity conditions they are strongly accelerated by buoyancy forces and rise through the channel following either helical or zig-zag trajectories [36]. In their path, they drag the liquid on their surroundings, inducing velocity fluctuations that can be either dissipated by viscosity or strongly enhanced by cooperative interaction between collections of bubbles, up to scales of movement much larger than the size of the bubble, thus creating what is known as pseudo-turbulence [37]. The vertical injection of bubbles creates roughly cylindrical columns of rising bubbles that interact strongly and follow complex oscillatory rising paths. The strong buoyancy forces and the pseudo-turbulence generated in the neighborhood of the bubbles, confine them in these columns regardless of the degree of turbulence inherent in the duct co-flow.

Once the buoyancy is switched off, bubbles quickly decelerate and relax to the local liquid flow velocity within their viscous relaxation time. In a time scale of the order of T_c, the flow becomes more homogeneous and bubbles spread to fill the whole channel. Even though some remnants of the pseudo-turbulence may have longer relaxation times, the time scale of
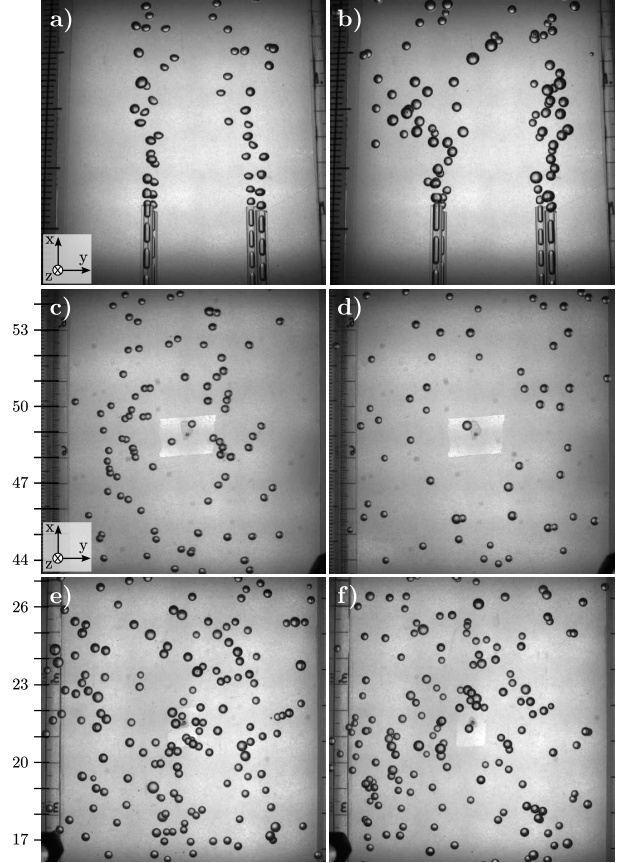
the experiment is sufficient to observe the emergence of a steady regime dominated by the co-flow.

Figures 4 and 5 show two representative snapshots of the different aspects explained above for bubble sizes: $d_B = 1.6$ mm and 2.5 mm, respectively. For both figures, cases *a* and *b* compare the performance of the injectors in normal gravity and in microgravity. Case *c* shows the distribution of bubbles in normal gravity conditions. Despite that they have risen a distance of nearly 60 cm within a turbulent flow, it is easy to see how they still remain confined at the central part of the duct due to the buoyancy forces. Case *d* shows the distribution of bubbles at the same distance in microgravity conditions, after the spreading of bubbles takes place. Finally, cases *e* and *f* show the higher density of bubbles achieved when those that have been injected in microgravity reach the observation areas. That is because bubbles injected during normal gravity conditions, despite being generated at the same frequency by the T-junctions, acquire a finite velocity with respect to the carrying flow, due to buoyancy forces, implying that mean separation between bubbles is larger. On the contrary, bubbles injected in microgravity disperse to a density only dependent on the injection parameters, as previously seen in equation (3). Density is even bigger

#	Q_l (ml/min)	Q_g (ml/min)	$Q_{\text{co-flow}}$ (l/min)
D1	75	34	35
D2	30	16	35
D3	70	51	80
D4	70	51	35
D5	37	19	80
D6	70	46	35
D7	70	65	77
D8	70	46	81
D9	18	46	81
D10	70	46	81
D11	18	46	81

Table 2: Parameters of injection correspondent to the experimental drops used for the data analysis in the present work.

Figure 6: Profiles of mean velocity of bubbles $\langle u_x \rangle$ at various times of the experiment for a single realization (D8) with Re = 13000

Figure 7: Profiles of mean velocity of bubbles $\langle u_x \rangle$ averaged over the measures of 4 different cameras of two equivalent experiments (D8+D10) at Re = 13000, at various times of the experiment

in *f*, due to its slower co-flow.

3.3. Bubble velocity statistics

Particle tracking has been used to identify the paths described by all the bubbles in the recordings. The injection parameters for the cases analyzed here are listed in Table 2. For experiments of isolated bubbles it would be possible in principle to reconstruct their three-dimensional trajectory from the data extracted of the pair of video cameras that simultaneously film at perpendicular planes of the duct. In practice, however, this is not possible in our case due to the large number of bubbles, implying a high degree of screening and the inherent difficulty of matching the bubble identities in successive snapshots. Therefore we are not able to measure the components of position and velocity over the visual direction *z*, perpendicular to the pictures, but only over directions *x*, in the direction of the co-flow, and *y*, perpendicular to both the co-flow and the visual direction. In the data analysis it is thus necessary to take into account that local fields at positions (x, y) are in fact averaged quantities in regions that may include significantly differences, like regions far or near the sidewalls.

In the present case and to perform a statistical analysis of the bubble velocity in the duct we have averaged their velocity on each point over temporal intervals of 0.6 s (being $t = 0$ the beginning of microgravity). In addition to this, we have also averaged over the direction of the main flow (x), assuming it to be homogeneous for the relatively small distance contained in the observation field of one video camera (around 10 cm). Averages are then performed by partitioning the transverse (y) width into 10 intervals, so that a dependence of results on the *y* coordinate can be obtained.

Figure 6 shows the profiles of mean velocity of bubbles for a typical realization with Re = 13000 and bubble size $d_T = 1.6$ mm. The irregularities shown in those profiles are due to the poor statistics of the experimental averaging (note that the microgravity conditions for each experiment last only 4.7 s) and provide a grasp of the large velocity fluctuations taking place in a given realization of the flow, corresponding to the relatively high degree of turbulence. In order to obtain the regular profiles
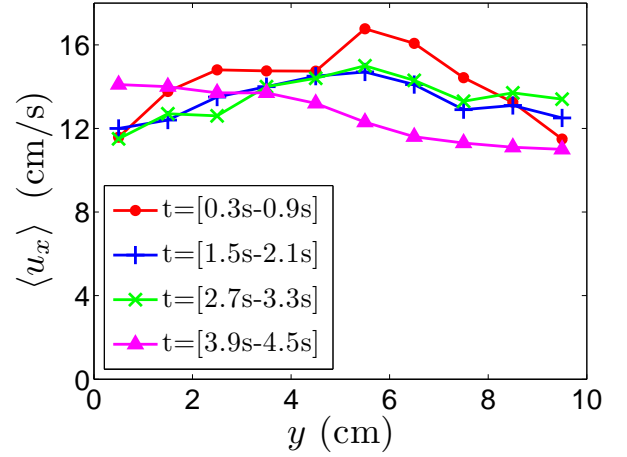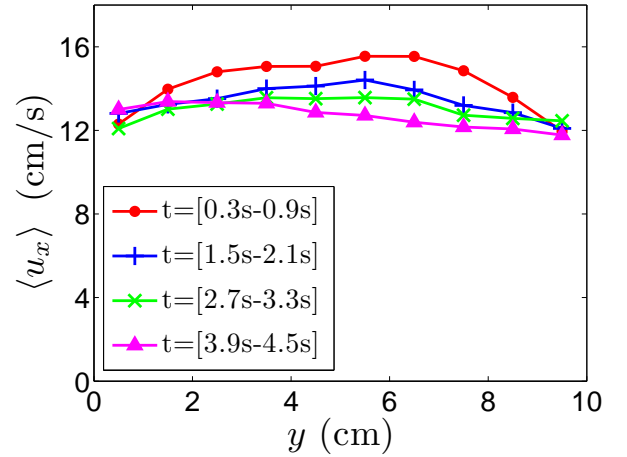
of mean velocity, we average the results over four equivalent realizations with the same characteristics. The resulting profiles of mean velocity and root-mean-square of velocity fluctuations are shown on Figures 7 and 8, respectively. In both figures it can be appreciated a decrease in time of their magnitudes, which is attributed to the decay of pseudo-turbulence, and hence constitutes a first rough characterization of the temporal evolution associated to the relaxation of the flow dragged by buoyancy forces prior to microgravity.

Due to the mentioned averaging over the visual direction, and given also the unavoidable limited replicability of an experiment and the large fluctuations inherent to the turbulence, it makes no sense to try to obtain averaged information on a local basis. Therefore we will compare the different cases by averaging out the spatial information into a single parameter for each profile. This averaging will be appropriately weighted using
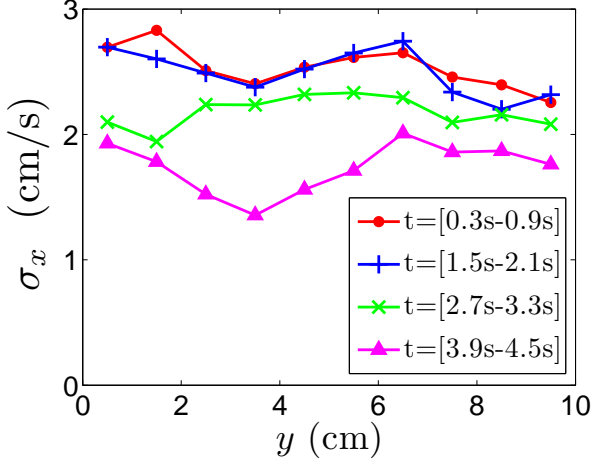
Figure 8: Profiles of velocity fluctuations σ_x of bubbles averaged over the measures of 4 different cameras of two equivalent experiments (D8+D10) at Re = 13000, at various times of the experiment
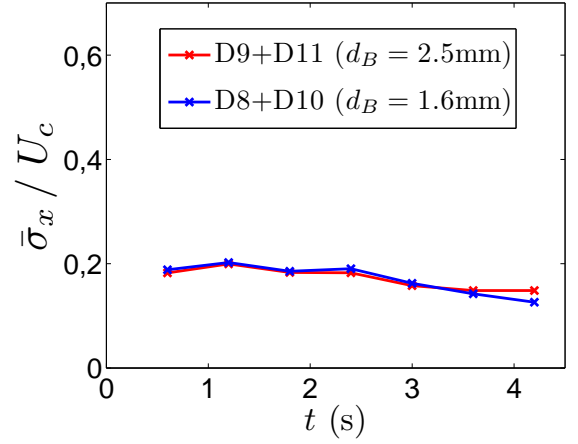

Figure 9: Relative velocity fluctuations for bubbles of size $d_B = 1.6$mm and 2.5mm. Each line has been averaged over the mesures of 4 cameras from two equivalent experiments at Re = 13000

information from the same experiments as follows,

$$\bar{u}_i = \frac{\sum_k \langle u_i(y_k) \rangle \, n(y_k)}{\sum_k n(y_k)} \, , \qquad (4)$$

$$\bar{\sigma}_i = \frac{\sum_k \sigma_i(y_k) \, n(y_k)}{\sum_k n(y_k)} \, , \qquad (5)$$

where $n(y_k)$ stands for the mean number of bubbles on each interval of the y direction for a given temporal period, and $\sigma_i^2 = \langle u_i^2 \rangle - \langle u_i \rangle^2$ is the variance of the i component of velocity. This averaging will reduce each profile into one characteristic parameter of the flow while granting prevalence of the information from the areas with larger number of bubbles, which are statistically more significant. This reduces the impact of the contributions closer to the sidewalls, while focusing on the central areas of the duct, where the flow is really mixed and fairly uniform and homogeneous. Note that we have used the mean density of bubbles instead of using the total number of velocity measurements since the latter are highly correlated in a single trajectory of a given bubble.

Results for relative velocity fluctuations are plotted in Fig. 9. They are obtained over the averaging of equivalent realizations with Re = 13000 for two different sizes of bubbles, but maintaining the injected gas void fraction constant, and normalized to the characteristic velocity U_c of the co-flow (i.e., its mean velocity, as measured by a flow-meter placed right after the pump). Results show no noticeable difference on the relative velocity dispersion for both sizes of bubbles, suggesting that bubble size does not play a significant role in this characterization of turbulence in our range of parameters.

3.4. Decay of pseudo-turbulence

The averaged velocity of bubbles as a function of time for several realizations with various injection parameters is pre-
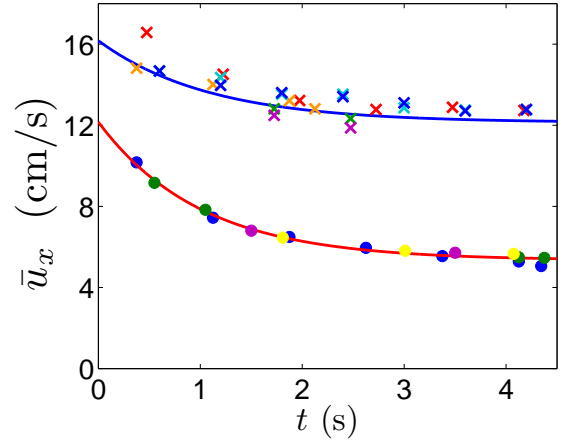

Figure 10: Evolution in time of the mean velocity of bubbles $\bar{u}_x$. Each color correspond to a different single experiment (see the legend in Fig 11). Exponential fittings in solid lines are described in Table 3.

sented in Figure 10. Here each color represents a different experiment. Circles stand for cases with co-flows with Re = 6000 while crosses correspond to Re = 13000.

Experimental values have been fitted to an exponential decay of the form

$$\bar{u}_x = \left(a + b e^{-t/\tau} \right) U_c \, , \qquad (6)$$

where a is the mean velocity of the stationary flow, b corresponds to the added mean flow at $t = 0$ due to the effect of buoyancy forces (both a and b are normalized in units of the characteristic velocity U_c) and τ is an effective relaxation time.

Observed decays are much slower than the scale τ_B associated to the relaxation of bubble velocity to the local flow velocity which, as seen on Eq. (2), depends on its size but it is $\tau_B < 0.2$ s for all the injection parameters studied in our experiments. Therefore the observed relaxation is interpreted as the decay of the local flows associated with pseudo-turbulence.

7

Param	Re	a	b	τ (s)
$\bar{u}_x$	6000	0.88	1.13	1.01
$\bar{u}_x$	13000	0.93	0.31	1.09
$\bar{\sigma}_x$	6000	0.10	0.43	3.2
$\bar{\sigma}_x$	13000	0.11	0.08	3.2
$\bar{\sigma}_y$	6000	0.13	0.21	2.4
$\bar{\sigma}_y$	13000	0.08	0.05	2.4

Table 3: Exponential fittings of the form $\bar{u}_x = \left(a + be^{-t/\tau}\right) U_c$, used in Fig.10 (for parameter $\bar{u}_x$) and Fig.11 (for parameters $\bar{\sigma}_x$ and $\bar{\sigma}_y$)

Table 3 shows that, in both cases of $\bar{u}_x$, the decay of pseudo-turbulence has a relaxation time $\tau \simeq 1$ s that is essentially independent from the Reynolds number of the carrying flow. That indicates that the remnants of pseudo-turbulence persist for a relatively long time after the relaxation of all bubbles to their local flow velocity.

Figure 11 shows our results on the relative velocity fluctuations. Each color denotes a specific experiment as in the previous figure. A first remarkable observation is that the experiments with smaller Reynolds numbers exhibit a larger value of the relative velocity fluctuations. Note that this would not be consistent with simple scaling arguments which, for fully developed turbulence, would suggest this observable to be essentially independent of Re. A more precise analysis must rely on numerical computation within the duct-flow geometry and with the actual flow parameters of experiments. We have carried out a Lattice-Boltzmann simulation of the duct flow with the experimental parameters (data not shown), and have explicitly checked that, within statistical uncertainty, the average profile of the relative velocity fluctuations at different sections of the flow appear essentially independent of Re for passive tracers. This analysis will be presented elsewhere [33, 38]. Consequently, our result points toward an active coupling of bubbles to the flow. It is worth remarking that since we are measuring velocities of bubbles while we have no tracers of the actual liquid flow, it is not possible to assert an actual modification of the statistics of the carrying flow due to the presence of bubbles. Strictly speaking we only observe that bubbles do not seem to be tracing the carrying flow as passive tracers.

A detailed analysis shows that for all the experiments with Re = 6000 (circles), fluctuations decay with a similar characteristic time and seem to relax to the same asymptotic value, even though the initial value of the velocity dispersion varies largely from experiment to experiment. We have not found any correlation of this initial dispersion with the injection parameters of bubbles. We can only attribute this effect to an inherent variability of the preparation of the initial condition, which cannot be fully controlled.

For cases with Re = 13000 (crosses), unlike those with smaller Reynolds number, pseudo-turbulence seems to have a minor effect into the velocity fluctuations. The fitting curves in the figures have been added to guide the eye through the evolution of the cloud of points. To define them, we have first fitted a relaxation time τ (which is the parameter that seems more robust) for each direction of a characteristic experiment, and then
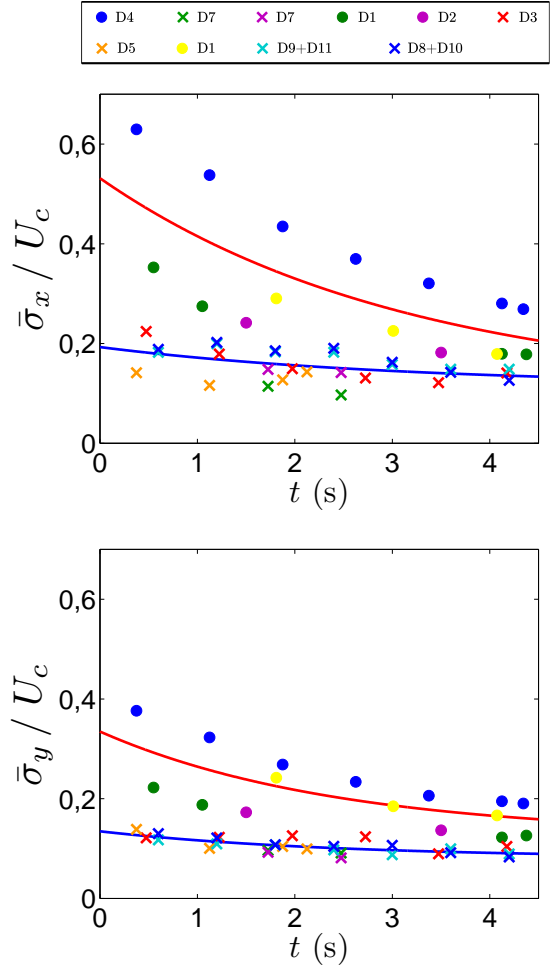

Figure 11: Relative bubble velocity fluctuations for several different experiments. Circles correspond at cases with Re = 6000, crosses are for Re = 13000. *(Left):* Fluctuations on the direction of the main flow. *(Right):* Fluctuations transversal to the main flow.

we have imposed these values of τ in the fitting of the rest of the data. The resulting curves are in Table 3. From these fittings it is interesting to observe the resulting relaxation times, $\tau = 3.2$ s and 2.4 s respectively. These are significantly larger than the values found for the relaxation of the mean velocity ($\tau = 1.0$ s), suggesting that velocity fluctuations of the pseudo-turbulence effectively decay to the co-flow values in a slower time scale than the mean velocity.

Finally, even though the asymptotic values of the relative fluctuations (parameter a in the fittings in Table 3) are subject to relatively larger uncertainty than the corresponding time scales, the transversal y-components show a significant dependence of their relative fluctuations on the Reynolds number, along the lines of the overall tendency to decrease for increasing Re. For the longitudinal components, however, the fitted asymptotic value does not exhibit any conclusive tendency in this respect.

4. Discussion and Conclusion

A new experimental setup for the generation and study of monodisperse bubble suspensions in microgravity has been designed, constructed and tested. The setup has been adapted to the mechanical requirements of ZARM Drop Tower facility in Bremen where 36 drops of 4.7 s of high quality microgravity ($< 10^{-5}g$) where conducted.

The experimental system has been designed to achieve homogeneous, monodisperse suspensions of spherical bubbles in a turbulent flow, with the capability to control separately the Reynolds number of the carrying flow, the size of the bubbles and the density of bubbles, within ranges of parameters that are relevant both to the fundamental study of turbulent two-phase dispersions and to potential applications in space technology. The method has been proven to be insensitive to gravity, and to be capable to achieve highly homogeneous suspensions with good control of the above three main physical parameters.

The method is based on a combination of several units of a previously developed T-junction capillary injector [22] where regular trains of bubble are created prior to injection. The bubble jets formed by each injector are then mixed by a turbulent carrying flow thus giving rise to a homogeneous. monodisperse bubble suspension. Reynolds numbers for the carrying flow with respect to the duct size of the order of Re = 6000 or larger have proved to be high enough to uniformly spread the bubble distribution. Efficient homogeneous spreading with minimal degree of bubble coalescence to maintain monodispersivity is typically achieved for bubble densities such that the mean bubble separation is of the order of the most energetic eddies of the flow, implying that the gas volume fraction is relatively small, of a few percent. However, the bubble size in our experiments was larger than the turbulent dissipative scale, implying that bubbles are not passive tracers but can potentially modify the carrying flow. Our range of parameters imply sufficiently small Weber numbers such that bubbles remain spherical. This is a convenient property to simplify the theoretical modeling of the bubble suspension.

The system proposed is sufficiently versatile to allow broader ranges of parameters than explored in the present proof-of-principle tests. Monodispersivity of bubbles can be achieved for sizes that are controlled by the diameter of the T-junction injectors, and for a fixed diameter it can be fine-tuned within a certain range controlling the gas and liquid injection rates [22]. The performance of the individual injectors is gravity-independent and has been characterized exhaustively in Refs. [22, 23, 24]. Once the single-jet parameters have been fixed, implying a given bubble size and frequency of bubble injection, the overall gas volume fraction injected in the carrying flow can be changed by varying the number of T-junction injectors. Finally the degree of turbulence of the carrying flow can be modified with the appropriate grid at the duct inlet, and controlling the total volumetric flow of liquid.

In addition to demonstrate and characterize the performance of the proposed setup in microgravity conditions, we have illustrated its use to collect relevant data for the study of turbulent bubble suspensions. High speed video recording at different positions downstream combined with particle tracking techniques have been used, for instance, to analyze the statistics of bubble velocity fluctuations. In particular, the drop-tower experimental protocol provides naturally a new way to approach to the study of pseudo-turbulence, since gravity can be switched off when a pseudo-turbulent bubble suspension is formed. Specifically, we have illustrated this possibility with a first quantitative characterization the decay time of pseudo-turbulence for different Reynolds numbers.

As another illustration we have quantified bubble velocity fluctuations and compared them with data obtained elsewhere from Lattice-Boltzmann simulations under the same conditions [33, 38]. A weak dependence observed on the relative bubble velocity fluctuations with Reynolds number that does not seem consistent with the Lattice-Boltzmann simulation data can be interpreted as a signature of an active coupling of bubbles with the flow even at the small volume fraction addressed.

Other interesting strategies to analyze particle-tracking data would be concerned with the space-time statistics of bubble pairs, and its comparison with that of passive tracers in simulations, with the aim at characterizing statistical properties of bubble trajectories and their implications for the probability of bubble coalescence and for the formation of bubble clusters. These possibilities have not been addressed here but have been discussed in Ref. [33].

To conclude, we would like to stress that the method here proposed and tested provides a very versatile tool to acquire valuable data on the physics of turbulent bubble suspensions in microgravity, by providing good control of a variety of parameters irrespectively of the actual acceleration environment. High-quality data of turbulent bubble flows in microgravity are usually scarce and difficult to obtain, due to the difficulty of bubble management in microgravity, and to the limited access to high quality microgravity environments. We hope that our method can contribute significantly to improve our understanding of fundamental aspects of this challenging problem, and that in turn it may eventually have practical relevance in space technology applications.

References

[1] S. Balachandar, J. Eaton, Turbulent dispersed multiphase flow, Annual Review of Fluid Mechanics 42 (2010) 111–133.

[2] Z. Lixing, Advances in studies on turbulent dispersed multiphase flows, Chinese Journal of Chemical Engineering 18 (6) (2010) 889–898.

[3] M. Cisse, E.-W. Saw, M. Gibert, E. Bodenschatz, J. Bec, Turbulence attenuation by large neutrally buoyant particles, Physics of Fluids (1994-present) 27 (6) (2015) 061702.

[4] M. Milanez, G. Naterer, G. Venn, G. Richardson, Volume averaged pressure interactions for dispersed droplet phase modeling of multiphase flow, AIAA journal 42 (5) (2004) 973–979.

[5] F. Mashayek, Simulations of reacting droplets dispersed in isotropic turbulence, AIAA journal 37 (11) (1999) 1420–1425.

[6] C. M. Coimbra, R. Rangel, Spherical particle motion in harmonic stokes flows, AIAA journal 39 (9) (2001) 1673–1682.

[7] K. Sridhar, B. Chao, S. Soo, Pressure drop in fully developed, turbulent, liquid-vapor annular flows in zero gravity, AIAA journal 30 (4) (1992) 1016–1026.

[8] K. Sridhar, B. Chao, Disperse phase motion in neutrally buoyant and zero-gravity pipe flows, AIAA journal 31 (12) (1993) 2382–2384.

[9] M. Meyer, L. Johnson, B. Palaszewsky, D. Goebel, H. White, D. Coote, In-space propulsion systems roadmap, National Aeronautics and Space Administration, 2010.

[10] S. Hill, C. Kostyk, B. Motil, W. Notardonato, S. Rickman, T. Swanson, Thermal management systems roadmap., National Aeronautics and Space Administration, 2010.

[11] K. Paiva, M. Mantelli, L. Slongo, Experimental testing of mini heat pipes under microgravity conditions aboard a suborbital rocket, Aerospace Science and Technology 45 (2015) 367–375.

[12] K. Hurlbert, B. Bagdigian, C. Carroll, A. Jeevarajan, M. Kliss, B. Singh, Human health, life support and habitation systems roadmap, National Aeronautics and Space Administration, 2010.

[13] E. Seedhouse, Martian Outpost: The Challenges of Establishing a Human Settlement on Mars, Springer-Praxis, 2009.

[14] B. Guo, D. W. Holder, J. T. Tester, Two-phase oxidizing flow in a volatile removal assembly reactor under microgravity conditions, AIAA journal 43 (12) (2005) 2586–2592.

[15] T. Hibiki, T. Hazuku, T. Takamasa, M. Ishii, Interfacial-area transport equation at reduced-gravity conditions, AIAA journal 47 (5) (2009) 1123–1131.

[16] V. Bertola, E. Cafaro, Slug frequency measurement techniques in horizontal gas-liquid flow, AIAA journal 40 (5) (2002) 1010–1012.

[17] H. K. Kytömaa, Stability of the structure in multicomponent flows, Ph.D. Thesis. California Institute of Technology., 1987.

[18] G. Tryggvason, J. Lu, S. Biswas, A. Esmaeeli, Studies of bubbly channel flows by direct numerical simulations, Conference on Turbulence and Interactions TI2006.

[19] I. M. Mazzitelli, D. Lohse, F. Toschi, The effect of microbubbles on developed turbulence, Physics of fluids 15 (1) (2003) L5–L8.

[20] C. Colin, D. Legendre, J. Fabre, Bubble distribution in a turbulent pipe flow, First International Symposium on Microgravity Research and Applications in Physical Sciences and Biotechnology. ESA SP-454.

[21] J. M. Gordillo, Z. Cheng, A. M. Ganan-Calvo, M. Márquez, D. A. Weitz, A new device for the generation of microbubbles, Physics of Fluids 16 (8) (2004) 2828–2834.

[22] J. Carrera, X. Ruiz, L. Ramírez-Piscina, J. Casademunt, M. Dreyer, Generation of a monodisperse microbubble jet in microgravity, AIAA Journal 46 (8) (2008) 2010 – 2019.

[23] S. Arias, X. Ruiz, J. Casademunt, L. Ramírez-Piscina, R. González-Cinca, Experimental study of a microchannel bubble injector for microgravity applications, Microgravity Science and Technology 21 (1-2) (2009) 107–111.

[24] S. Arias, R. González-Cinca, X. Ruiz, L. Ramírez-Piscina, J. Casademunt, Characterization of the performance of a minibubble generator in conditions relevant to microgravity, Colloids and Surfaces A: Physicochemical and Engineering Aspects 365 (1) (2010) 52–55.

[25] S. Arias, D. Legendre, R. González-Cinca, Numerical simulation of bubble generation in a T-junction, Computers & Fluids 56 (2012) 49–60.

[26] S. Arias, R. González-Cinca, Experimental analysis of the bubble–slug transition in a flow generated by a T-junction in a minichannel with air/water and air/ethanol mixtures in conditions relevant to microgravity, Chemical engineering science 91 (2013) 5–10.

[27] P. Bitlloch, X. Ruiz, L. Ramírez-Piscina, J. Casademunt, Turbulent bubble jets in microgravity. Spatial dispersion and velocity fluctuations, Micro-gravity Science and Technology 27 (3) (2015) 207–220.

[28] S. Arias, A. Montlaur, Numerical study and experimental comparison of two-phase flow generation in a T-junction, AIAA Journal.

[29] S. Mendez-Diaz, R. Zenit, S. C. Vicent, J. L. Muñoz-Cobo, A. Morales-Fuentes, Pseudoturbulence in bubbly and transition flow regimes, in: Fluid Dynamics in Physics, Engineering and Environmental Applications, Springer, 2013, pp. 217–224.

[30] J.-H. Chen, J.-S. Wu, G. Faeth, Turbulence generation in homogeneous particle-laden flows, AIAA journal 38 (4) (2000) 636–642.

[31] K. Lee, G. Faeth, J.-H. Chen, Properties of particle-generated turbulence in the final-decay period, AIAA journal 41 (7) (2003) 1332–1340.

[32] G. Riboux, F. Risso, D. Legendre, Experimental characterization of the agitation generated by bubbles rising at high reynolds number, Journal of Fluid Mechanics 643 (2010) 509–539.

[33] P. Bitlloch, Turbulent bubble suspensions and crystal growth in microgravity. Drop tower experiments and numerical simulations, PhD Thesis, 2012.

[34] A. Gosselin, S. Kranc, Underexpanded jets of liquid-gas bubble mixtures, AIAA Journal 9 (8) (1971) 1645–1646.

[35] M. Maxey, E. Chang, L. Wang, Interactions of particles and microbubbles with turbulence, Experimental Thermal and Fluid Science 12 (1996) 417–425.

[36] K. Wichterle, K. Smutná, M. Večeř, Shape and rising velocity of bubbles, Proceedings of the 36th International Conference of Slovak Soc.of Chem. Eng.(SSCHE).

[37] I. M. Mazzitelli, D. Lohse, Evolution of energy in flow driven by rising bubbles, Physical Review E 79 (066317).

[38] P. Bitlloch, X. Ruiz, L. Ramírez-Piscina, J. Casademunt, Velocity fluctuations in Lattice-Boltzmann simulations of turbulent duct flows, Unpublished.